Anisotropy of Assemblies of Densely Packed Co-Alloy Nanoparticles Embedded in Carbon Nanotubes

Serghej L Prischepa, Alexander L Danilyuk, Andrei V Kukharev, Costel Sorin Cojocaru, Nikolai I Kargin, François Le Normand

IEEE MAGNETICS LETTERS, Volume 10 (2019), 1-5

Anisotropy of Assemblies of Densely Packed Co-Alloy Nanoparticles Embedded in Carbon Nanotubes

Serghej L. Prischepa[1,2], Alexander L. Danilyuk[1], Andrei V. Kukharev[1,3], Costel S. Cojocaru[4,5], Nikolai I. Kargin[2], and Francois Le Normand[4,6]

[1] *Belarusian State University of Informatics and Radioelectronics, Minsk 220013, Belarus*
[2] *National Research Nuclear University "MEPhI," Moscow 115409, Russia*
[3] *Siberian Federal University, Krasnoyarsk 660041, Russia*
[4] *Institut de Physique et Chimie des Matériaux de Strasbourg, CNRS-University of Strasbourg, Strasbourg 67037, France*
[5] *LPICM Laboratory, Ecole Polytechnique/CNRS, Palaiseau Cedex 91128, France*
[6] *ICube/MaCEPV Laboratory, CNRS-University of Strasbourg, Strasbourg Cedex 67037, France*

Abstract—We report on the magnetic properties of an array of binary metal CoFe, CoNi, and CoPt nanoparticles (NPs) embedded inside vertically oriented carbon nanotubes (CNTs). Samples were synthesized by chemicalvapor deposition activated by current discharge plasma and hot filaments. Assemblies of Co-based catalytic NPs were prepared on Si/SiO_2 substrates by sputtering ultrathin films followed by reduction in an H_2/NH_3 mixture. As a result of the CNT growth, each CNT contained only one ferromagnetic NP located at the top. For all samples, the easy axis of magnetization was along the CNT axis. The magnetic parameters, including effective anisotropy constant and the contributions of dipole interactions and shape, magnetocrystalline, and magnetoelastic anisotropies, were estimated based on the experimental data and a random-anisotropy model. The magnetoelastic contribution was decisive. From the magnetoelasticity, the stresses in the NPs embedded in the CNTs were determined. Finally, the magnetization distribution in CoFe, CoNi, and CoPt NPs was simulated considering the magnetoelastic contribution.

Keywords : Nanomagnetics, ferromagnetic binary metal nanoparticles, magnetoelastic anisotropy.

I. INTRODUCTION

Magnetic nanoparticles (**NP**s) have attracted tremendous interest in various fields due to their unique properties and promising applications [Srikanth 2019]. Employing NPs for magnetic data storage could lead to significant advancement in storage density and higher total capacity. Single-domain NPs are characterized by single magnetic moment with a direction adjusted by local anisotropy. The stability of the magnetization with time depends on the relation between thermal energy and total anisotropy energy of the NP, $K_{\text{eff}}V$, where K_{eff} is the total effective anisotropy energy density and V is the volume of NP. With a noticeable decrease in V, the contribution of K_{eff} to this product should increase in order to maintain thermal stability. The K_{eff} is generally the superposition of magnetocrystalline (K_{MC}), shape (K_S), and magnetoelastic (K_{ME}) energies. If K_{MC} does not exceed 10^4–10^5 J/m^3 for 3d metals (Fe, Ni, Co), the K_S, which is proportional to the square of the saturation magnetization M_S^2, could reach values of 10^6 J/m^3. Finally, in nanostructured materials plastic deformations are constrained by surfaces and interfaces. As a result, these materials may have significant elastic stresses. The contribution of K_{ME} becomes decisive if elastic stresses of the order of 1–10 GPa are reached.

To form a densely packed array of ferromagnetic NPs, prevent their agglomeration, and achieve long-time protection against external environment, one of the best ways is to embed them into the carbon nanotubes (**CNT**s) [Grobert 1999, Leonhardt 2003, Baaziz 2012, Ghunaim 2018a]. Selective introducing into the inner channel of multiwalled CNTs could give rise to a new family of hybrid materials with novel functionality, which can find applications in magnetoelectronics. Generally, CNTs are synthesized by different methods [Purohit 2014]. The common characteristic of all techniques is to provide energy to a carbon source for the creation of carbon atoms that generate CNTs. Chemical vapor deposition (**CVD**), which involves carbon decomposition of organic precursors over 3d catalytic metals, is one of the best techniques to synthesize CNTs and to fill them by ferromagnetic NPs. In this method, the decomposition of the carbon precursor and CNT formation take place on the surface of catalyst particles. CNTs can be produced at relatively low temperatures, and their size can be controlled by varying the size of catalyst particles. Many efforts have been performed by different groups to improve the reliability and reproducibility of CVD for optimum CNT growth [Jourdain 2013, Allaedini 2016]. For magnetoelectronics, it is important that this method allows synthesizing the vertically aligned macroscopically large areas of CNTs.

One of the routes to achieve an increased magnetic anisotropy in NPs is the synthesis of binary alloys rather than unary metal NPs. Multicomponent ferromagnetic NPs is an active field of research where alloying, crystalline structure, and stresses can vastly alter their magnetic properties [Rohart 2006, Seo 2006, Marusak 2017]. Successful experiments on the CNT filling by alloyed FeNi [Lv 2008], FeCo [Lv 2008, Ghunaim 2018b], FePd [Boi 2015], and FeGa [Ghunaim 2018a] NPs are known. FePt was introduced into fullerene-like carbon nano-onions [Boi 2017]. In all these experiments, the number of NPs

Corresponding author: Serghej L. Prischepa (e-mail: prischepa@bsuir.by).
Digital Object Identifier 10.1109/LMAG.2019.2933380

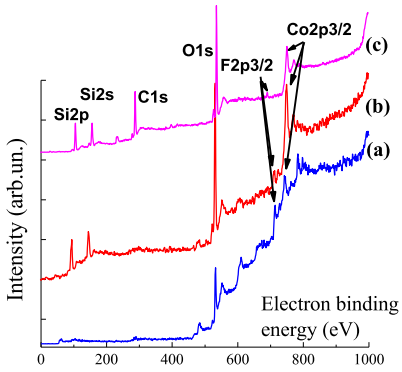

Fig. 1. XPS spectra of CoFe samples (a) before, (b) after the reduction, and (c) after the CNT growth.

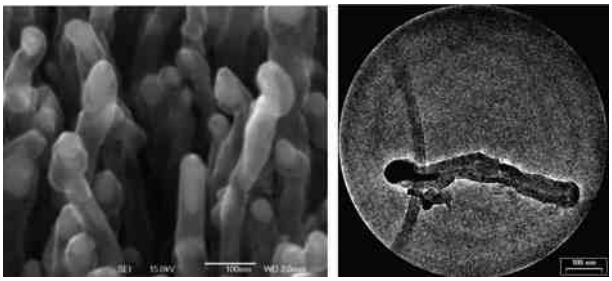

Fig. 2. (Left) SEM and (right) TEM images of CNTs grown on CoPt.

in one CNT was usually much more than one. Recently, it has been demonstrated that it is possible to embed only one Co NP in each CNT belonging to the array of closely packed vertically aligned nanotubes [Prischepa 2019]. Such samples synthesized by CVD activated by current discharge plasma and hot filaments have perpendicular magnetic anisotropy due to combination of *hcp* crystalline lattice and large elastic stresses caused by peculiar CNT growth and NP's morphology [Prischepa 2019]. In this letter, we continue to develop this approach (to fill each CNT with only one NP) and use Co binary alloys (CoFe, CoNi, CoPt) as catalytic NPs for CNT growth. The choice of these binary compounds is due to the following reasons. First, they are applicable as a catalyst for CNT growth. Binary metal NPs are more reliable catalysts than unary for the CNT growth because two metals can enhance certain functions by playing complementary catalytic roles [Allaedini 2016]. Second, each of this binary metal is a ferromagnet with its characteristic features of magnetic properties. CoFe alloys have the highest saturation magnetization (M_S–240 emu/g) among this class of materials, which is important for magnetic data storage application and magnetic resonance imaging[Bader 2006, Seo 2006]. However, this alloy is chemically unstable, which makes the synthesis of robust CoFe NPs extremely challenging. CoNi, *vice versa*, is a very chemically stable alloy [Marusak 2017] and could possess a high magnetocrystalline anisotropy. Therefore, it is considered as a promising candidate for the next generation of magnetic storage media and high-performance permanent magnets [Zeng 2002]. Finally, CoPt NPs have attracted recently considerable attention due to high coercivity, saturation magnetization, and magnetocrystalline anisotropy [Rohart 2006].

II. SAMPLES

Samples were fabricated on Si(100)/SiO_2(8 nm) substrates. First, Co and either Fe, Ni, or Pt were cosputtered in Ar atmosphere with the deposition rates of 0.06, 0.04, 0.05, and 0.04 nm/s, respectively. The nominal thickness was 9 nm for Co and 4 nm for other metals. The obtained films were reduced to NPs at 973 K in a flux of H_2:NH_3 = 1:4. The obtained array of metallic NPs was afterward used for the CNT growth. It was possible to analyze samples by X-ray photoelectron spectroscopy (**XPS**) at each step of the fabrication process without exposure to air [Le Normand 2007, Danilyuk 2018]. In Fig. 1, we present the XPS survey spectra of a CoFe sample before [see Fig. 1(a)], after the reduction [see Fig. 1(b)] and after the CNT growth [see Fig. 1(c)]. The appearance of Si2p, Si2s, and O1s lines after the reduction is caused by the presence of these materials in the surface substrate while they were entirely covered by the metallic films initially. This confirms the formation of noncontinuous metallic NPs. After the NPs formation, the sample was *in situ* subjected to the CNT growth. For that, we inject into the reactor the mixture of H_2 (80%) and C_2H_2 (20%) at P = 15 mbar activated by current discharge plasma and hot filament. More details about this technique can be found in Cojocaru [2006] and Danilyuk [2018]. In the XPS survey spectrum after the CNT growth, a noticeable peak C1s of carbon appears. The presence of both Si and SiO_2 peaks indicate the absence of continuous carbon film on the substrate. From the result of Fig. 1(c), it is possible to quantitatively analyze the relation between Co and Fe by means of intensity ratio of Co $2p_{3/2}$ and Fe $2p_{3/2}$ lines (not shown here) employing the standard software CasaXPS. We got an atomic ratio Fe/Co = 0.54 with Fe and Co both at the Fe0 and Co0 states, mainly. Similar studies have been conducted for CNT grown on CoNi (Ni $2p_{3/2}$) and CoPt (Pt $4f_{7/2}$). The obtained atomic ratios are then Ni/Co = 0.05 and Pt/Co = 0.05. The spreading in the alloying of these transition metals with Co obtained by XPS must be interpreted with caution; however, as the sensitivity of the XPS measurements is around 5 nm and the CNT thickness strongly depends on the alloy used but can be much thicker than 5 nm (see Fig. 2). Other parameters can explain these results as the catalytic affinity of these metals to C, which is higher for Co or Fe than for Ni or Pt. This is consistent with the highest catalytic activity of them with respect to the growth of carbon nanotubes [Allaedini 2016].

After analyzing the chemical composition, we performed electron microscopy study to determine the orientation and the regularity of the CNT arrays. In Fig. 2, we show the scanning electron microscopy (**SEM**) and transmission electron microscopy (**TEM**) images of CNTs on CoPt NPs. It follows that CNTs are vertically oriented and catalytic NP is located at the top of each CNT. It should be emphasized that the major part of catalytic NPs is anisotropic, as it shown in Fig. 2 with the long axis parallel to the nanotube axis. Some of the NPs present a nailheadlike morphology. This form is shown in the TEM image (see Fig. 2, right-hand side). The diameter of the NPs is determined by the diameter of the inner CNT channel and was equal to approximately 20 nm with a length of about 100 nm. Estimated from the SEM images density of CNTs was equal to (2.5–3.5) × 10^{10} cm^{-2}, and their height was about 400 nm. There is a certain variation in the height of nanotubes, which seems to be associated with both different sizes of NPs and variations in their chemical composition. The crystal structure of the deposited Co NPs was tested by selective area electron diffraction (**SAED**) [Prischepa 2019]. Since it is quite difficult to

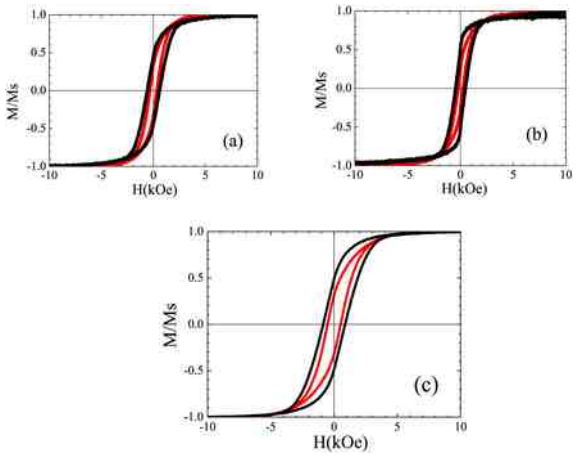

Fig. 3. $M(H)$ curves for the parallel (red) and perpendicular (black) magnetic field orientations. T= 300 K. (a) Sample CNT grown on CoFe. (b) Sample CNT grown on CoNi. (c) Sample CNT grown on CoPt.

make a single crystal structure by sputtering, it was logical to observe a mixture of cubic and hexagonal Co lattices [Prischepa 2019]. Small amounts of both Ni and Pt (≤ 15%) do not change the crystal lattice of Co [Handbook 1996], whereas 35% of Fe in CoFe leads to stabilization of the *fcc* lattice and to the absence of the *hcp* one [Skomski 1999]. Therefore, we suppose that in CoNi and CoPt NPs, we still have a mixture of *fcc* and *hcp* lattices and in CoFe NPs only the *fcc* lattice is present. More work is in progress to unravel this point.

The reproducibility of the elaborated method is assured both by the plasma-enhanced CVD and accuracy in the metal deposition. Precise control of the parameters of the plasma process and the thickness of the deposited metal films leads to reproducibility in determining the atomic ratio.

III. RESULTS AND DISCUSSION

As clearly demonstrated by Danilyuk [2018], by atomic-force microscopy (**AFM**), and magnetic-force microscopy (**MFM**), Co NPs on the Si/SiO_2 substrate are strongly coupled forming large magnetic domains each of which contains about 100 NPs. MFM images of Co NPs on the top of CNTs revealed a unique correlation between the geometrical sizes of particles and the size of magnetic domains, each NP corresponding to a single domain [Danilyuk 2018]. For Co-based binary compounds, the result is similar. AFM-MFM images of the same area of CNTs grown on Co-alloy NPs have identical topography (not shown). Data were acquired on the samples with no magnetic exposure.

In Fig. 3, we show the magnetic hysteresis loops of CNTs grown on Co-based NPs measured at 300 K. Data are both for parallel and perpendicular orientations of magnetic field. Orientation was determined relative to the substrate's surface. These measurements are in good agreement with the MFM data. The preferential orientation of the easy axis is along the CNT axis despite the very high density of the NPs. This causes higher squareness M_R/M_S for the perpendicular field. The extracted from the $M(H)$ curves parameters for binary metal NPs together with the data for Co [Danilyuk 2018] are presented in Table 1. It is seen that for CoPt, coercivity reaches the maximum

Table 1. Squareness and coercivity of different samples.

NP	M_R/M_S perp	M_R/M_S par	H_c (kOe) perp	H_c (kOe) par
Co	0.38	0.18	0.77	0.30
CoFe	0.44	0.33	0.58	0.36
CoNi	0.52	0.30	0.43	0.25
CoPt	0.50	0.32	0.92	0.54

Table 2. Magnetic anisotropy contributions.

Parameter	Co	CoFe	CoNi	CoPt
K_{eff}, J/m^3	2.73×10^5	2.15×10^5	2.24×10^5	2.99×10^5
K_{MC}, J/m^3	2.05×10^5	0.45×10^5	1.53×10^5	3.9×10^5
K_{DD}, J/m^3	1.09×10^5	1.57×10^5	1.09×10^5	0.98×10^5
K_S, J/m^3	-6.16×10^5	-8.87×10^5	-6.16×10^5	-5.56×10^5
K_{ME}, J/m^3	5.75×10^5	9×10^5	5.78×10^5	3.67×10^5

values. The squareness values increase for all the binary Co-based alloyed NPs with respect to pure Co, whereas the coercivity is greater only with CoPt alloy NPs.

The tendency to perpendicular anisotropy is associated not only with the changed shape of NPs after the CNT growth, but also with possible elastic stresses arising in NPs during the growth of CNTs on them. The effective anisotropy constant K_{eff} could be evaluated within the random anisotropy model (**RAM**) [Löffler 1998] that can be successfully applied for the analysis of magnetically functionalized CNTs [Danilyuk 2015]. The obtained values are summarized in Table 2. On the basis of the obtained K_{eff} values, and taking advantage of the fact that for NPs on the substrate (before the CNT growth) magnetoelasticity and shape anisotropy can be neglected, it is possible to evaluate the contributions of all components (K_{MC}, K_S, K_{ME}, dipole interaction K_{DD}) to the magnetic anisotropy. This approach is described in detail by Danilyuk [2018]. Here, we should only emphasize that the K_{MC} value that was previously estimated for NPs on Si/SiO_2 substrate was supposed to be the same for NPs after the CNT growth. The obtained various anisotropy contributions are summarized in Table 2.

It follows that the main contribution to the anisotropy for CoFe, CoPt, and CoNi is due to shape and elastic stresses. In CoPt, magnetocrystalline anisotropy also is decisive. As we mentioned before, we reasonably suppose that for CoNi and CoPt, two crystal lattices, *fcc* and *hcp*, should be considered. The smallest K_{MC} for CoFe reflects the fact that for high iron concentration, CoFe lattice becomes *fcc* [Skomski 1999]. It is worth underlining that varying the content of the second metal in Co, it is possible to tune not only the K_{MC} value, but also the magnetoelasticity as the elastic stresses σ in Co are affected significantly by the type of the crystal lattice [Sander 1999]. For that reason, we estimated the σ values in our binary metal NPs. For *fcc* lattice, the K_{ME} is expressed as

$$K_{ME}^{fcc} \approx -(3/2)\lambda\sigma \qquad (1)$$

where λ is the magnetostriction constant. For *fcc* Co, the value of $\sigma \approx$ 7 GPa was obtained [Danilyuk 2018]. For *fcc* CoFe, this approach leads to slightly greater stresses, $\sigma \approx 8$ GPa. For *fcc*, CoNi and CoPt stresses are equal to 5 and 3.7 GPa, respectively.

For *hcp* lattice, the result depends on the orientation of the hexagonal axis [0001] with respect to the CNT axis. If the hexagonal axis is

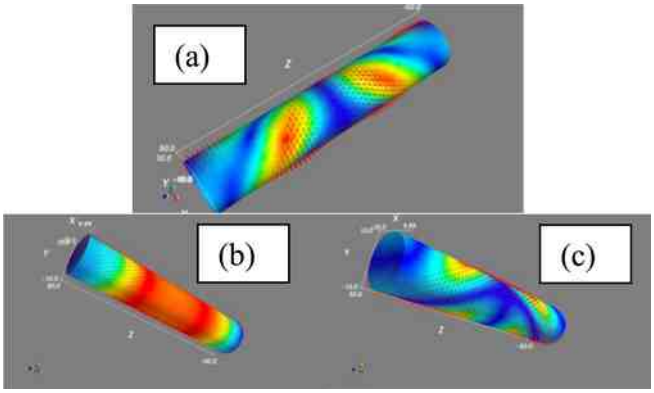

Fig. 4. Relaxed magnetization configuration of *fcc* CoFe at. (a) σ = 5 GPa and *hcp* CoPt for parallel. (b) σ = 10 GPa. (c) Perpendicular, σ = 5 GPa hexagonal axis orientation with respect to the CNT axis. Red and blue colors correspond to the orientation of the magnetization along and perpendicular to the nanocylinder, respectively.

parallel to the CNT, the K_{ME} is [Lee 1990]

$$K_{\mathrm{ME}}^{hcp} = -\left(c_{11} + c_{12} - \frac{2c_{13}^2}{c_{33}}\right)\left(\lambda_A + \lambda_B\right)\varepsilon_1 = \sigma\left(\lambda_A + \lambda_B\right) \quad (2)$$

where c_{ij} are elastic stiffness constants, the indices $i, j = 1, 2, 3$ number the axis of the hexagonal crystal (index 3 corresponds to the axis [0001]), λ_A and λ_B are magnetostriction constants, and ε_1 is the strain. For pure Co, the elastic stress is $\sigma \approx 3.4$ GPa [Danilyuk 2018]. In CoNi and CoPt, the obtained stresses were estimated as 5 GPa. For these calculations, we used parameters of *hcp* Co.

For the hexagonal axis aligned along the radial CNT direction, the exact expression for the K_{ME}^{hcp} depends on the orientation of crystal magnetization m [Sander 1999]

$$K_{\mathrm{ME}}^{hcp}(m) = \gamma\left(B_1\varepsilon_1 + B_2\varepsilon_3 + B_3(\varepsilon_1 + \varepsilon_2)\right) \quad (3)$$

where parameter γ depends on the direction cosines of the magnetization with respect to the [0001] axis, and B_i are magnetoelastic coupling coefficients. The largest stresses occur when the hexagonal axis is oriented along the magnetic field. For Co NPs in this case $\sigma \approx -11.3$ GPa [Danilyuk 2018], whereas for CoNi and CoPt, we obtained in this letter $\sigma \approx -10$ GPa. The minus sign indicates the compression stress.

On the basis of the above-mentioned parameters, it is possible to simulate the magnetic structure of the binary metal NPs inside CNTs. For that, we applied the Nmag package based on Landau–Lifshitz–Gilbert equation and finite-element methods [Danilyuk 2018]. The discretization length was selected as 2 nm. The size of the NP was assumed to be 100 nm in length and 20 nm in diameter, in accordance with the experimental data. Axis z is oriented along the nanocylinder axis. For the perpendicular orientation of the hexagon with respect to the CNT axis, the x-axis coincides with the [0001] axis of the *hcp* Co.

In Fig. 4(a), we show the relaxed magnetization configuration for *fcc* CoFe NP in the presence of σ = 5 GPa. One can see the essential nonhomogeneous magnetization. We should emphasize that in the absence of stress, the magnetization is homogeneous and is oriented along the CNT axis, like for pure Co [Danilyuk 2018]. The nonhomogeneous magnetization reduces the overall anisotropy of the sample causing convergence tendency of the hysteresis loops measured for different magnetic field orientations (see Fig. 3). The results for *fcc* CoNi and CoPt are similar.

In Fig. 4(b), we show the magnetization of the *hcp* CoPt NP for the parallel orientation of the [0001] axis at σ = 10 GPa. It follows from this result that the magnetization at such high stress is uniform in the central part of the NP. When the hexagonal axis is oriented perpendicular to the CNT axis, the magnetization becomes essentially nonhomogeneous even at lower σ. In Fig. 4(c), we present this result of the simulations for σ = 5 GPa. The results for *hcp* CoNi are similar.

From the obtained relaxed magnetization configurations, we may conclude that the perpendicular anisotropy in our samples is mostly due to the *hcp* crystal lattice of Co, which is preserved for low concentrations of the second metal. When, like in the case of CoFe, the lattice is *fcc*, the anisotropy reduces. For *hcp* lattice, the orientation of the hexagonal lattice has the greatest impact on the anisotropy. For the hexagonal axis oriented along the CNT one, the magnetization is highly uniform, which should reflect in high perpendicular anisotropy. The hexagonal axis oriented perpendicular to the CNT axis causes the nonhomogeneous NP magnetization and, as a result, lower anisotropy. The obtained results could pave a way for nanoengineering of densely packed magnetically isolated NPs with high perpendicular anisotropy, which is important for high-density recording.

ACKNOWLEDGMENT

The work of S. L. Prischepa was supported by the "Improving of the Competitiveness" Program of the National Research Nuclear University MEPhI – Moscow Engineering Physics Institute. The authors thank Prof. S. Colis (IPCMS, GEMM) for magnetic measurements.

REFERENCES

Allaedini G, Tasirin S M, Aminayi P, Yaakob Z, Talib M Z M (2016), "Carbon nanotubes via different catalysts and the important factors that affect their production: A review on catalyst preferences," *Int. J. Nano Dimension*, vol. 7, pp. 186–200, doi: 10.7508/ijnd.2016.03.002.

Baaziz W, Begin-Colin S, Pichon B P, Florea I, Ersen O, Zafeiratos S, Barbosa R, Begin D, Pham-Huu C (2012), "High-density monodispersed cobalt nanoparticles filled into multiwalled carbon nanotubes," *Chem. Mater.*, vol. 24, pp. 1549–1551, doi: 10.1021/cm300293b.

Bader S D (2006), "Colloquium: Opportunities in nanomagnetism," *Rev. Mod. Phys.*, vol. 78, pp. 1–15, doi: 10.1103/RevModPhys.78.1.

Boi F S, Guo J, Lan M, Xiang G, Wang S, Wen J, Zhang S (2015), "Synthesis of planar-graphite structures with embedded $Fe_{(x)}Pd_{(x)}$ or CoPd-$CoPd_2$ phases and of carbon nanotubes filled with $Fe_{(x)}Pd_{(x)}$ with variable filling ratio," *Carbon*, vol. 95, pp. 634–639, doi: 10.1016/j.carbon.2015.08.095.

Boi F S, Zhang X, Ivaturu S, Liu Q, Wen J, Wang S (2017), "UV absorption investigation of ferromagnetically filled ultra-thick carbon onions, carriers of the 217.5 nm Interstellar Absorption Feature," *J. Appl. Phys.*, vol. 122, 224305, doi: 10.1063/1.4999461.

Cojocaru C S, Le Normand F (2006), "On the role of activation mode in the plasma- and hot-filaments-enhanced catalytic chemical vapour deposition of vertically aligned carbon nanotubes," *Thin Solid Films*, vol. 515, pp. 53–58, doi: 10.1016/j.tsf.2005.12.137.

Danilyuk A L, Komissarov I V, Labunov V A, Le Normand F, Derory A, Hernandez J M, Tejada J, Prischepa S L (2015), "Manifestation of coherent magnetic anisotropy in a carbon nanotube matrix with low ferromagnetic nanoparticle content," *New J. Phys.*, vol. 17, 023073, doi: 10.1088/1367-2630/17/2/023073.

Danilyuk A L, Kukharev A V, Cojocaru C S, Le Normand F, Prischepa S L (2018), "Impact of aligned carbon nanotubes array on the magnetostatic isolation of closely packed ferromagnetic nanoparticles," *Carbon*, vol. 139, pp. 1104–1116, doi: 10.1016/j.carbon.2018.08.024.

Ghunaim R, Eckert V, Scholz M, Gellesch M, Wurmehl S, Damm C, Büchner B, Mertig M, Hampel S (2018a), "Carbon nanotube-assisted synthesis of ferromagnetic Heusler nanoparticles of Fe_3Ga (Nano-Galfenol)," *J. Mater. Chem. C*, vol. 6, pp. 1255–1263, doi: 10.1039/c7tc04618a.

Ghunaim R, Scholz M, Damm C, Rellinghaus B, Klingeler R, Büchner B, Mertig M, Hampel S (2018b), "Single-crystalline FeCo nanoparticle-filled carbon nanotubes: Synthesis, structural characterization and magnetic properties," *Beilstein J. Nanotechnol.*, vol. 9, pp. 1024–1034, doi: 10.3762/bjnano.9.95.

Grobert N, Hsu W K, Zhu Y Q, Hare J P, Kroto H W, Walton D R M, Terrones, M, Terrones, H, Redlich, Ph, Rühle, M, Escudero, R, and Morales, F (1999), "Enhanced magnetic coercivities in Fe nanowires," *Appl. Phys. Lett.*, vol. 75, pp. 3363–3365, doi: 10.1063/1.125352.

Jourdain V, Bichara C (2013), "Current understanding of the growth of carbon nanotubes in catalytic chemical vapour deposition," *Carbon*, vol. 58, pp. 2–39, doi: 10.1016/j.carbon.2013.02.046.

Le Normand F, Cojocaru C S, Fleaca C, Li J Q, Vincent P, Pirio G, Gangloff L, Nedellec Y, Legagneux P (2007) "A comparative study of the field emission properties of aligned films of carbon nanostructures, from carbon nanotubes to diamond," *Eur. Phys. J. Appl. Phys.*, vol. 38, pp. 115–127, doi: 10.1051/epjap:2007052.

Lee C H, He H, Lamelas F J, Vavra W, Uher C, Clarke R (1990), "Magnetic anisotropy in epitaxial Co superlattices," *Phys. Rev. B*, vol. 42, pp. 1066–1069, doi: 10.1103/PhysRevB.42.1066.

Leonhardt A, Ritschel M, Kozhuharova R, Graff A, Mühl T, Huhle R, Mönch I, Elefant D, Schneider S M (2003), "Synthesis and properties of filled carbon nanotubes," *Diamond Rel. Mater.*, vol. 12, pp. 790–793, doi: 10.1016/S0925-9635(02)00325-4.

Löffler J F, Meier J P, Doudin B, Ansermet J-P, Wagner W (1998), "Random and exchange anisotropy in consolidated nanostructure Fe and Ni: Role of grain size and trace oxides on the magnetic properties," *Phys. Rev. B*, vol. 57, pp. 2915–2924, doi: 10.1103/PhysRevB.57.2915.

Lv R, Kang F, Gu J, Gui X, Wei J, Wang K, Wu D (2008), "Carbon nanotubes filled with ferromagnetic alloy nanowires: Lightweight and wide-band microwave absorber," *Appl. Phys. Lett.*, vol. 93, 223105, doi: 10.1063/1.3042099.

Marusak K E, Johnston-Peck A C, Wu W C, Anderson B D, Tracy J B (2017), "Size and composition control of CoNi nanoparticles and their conversion into phosphides," *ACS Chem. Mater.*, vol. 29, pp. 2739–2747, doi: 10.1021/acs.chemmater.6b04335.

Okamoto, H, Schlesinger, Mark E, Mueller, E M, (1996), ASM Handbook of Alloy Phase Diagrams, vol. 3, Materials Park, OH, USA ASM 296 Int.

Prischepa S L, Danilyuk A L, Kukharev A V, Le Normand F, Cojocaru C S (2019), "Self-assembled magnetically isolated Co nanoparticles embedded inside carbon nanotubes," *IEEE Trans. Magn.*, vol. 55, 2300304, doi: 10.1109/TMAG.2018.2864692.

Purohit R, Purohit K, Rana S, Rana R S, Patel V (2014), "Carbon nanotubes and their growth methods," *Procedia Mater. Sci.*, vol. 6, pp. 716–728, doi: 10.1016/j.mspro.2014.07.088.

Rohart S, Raufast C, Favre L, Bernstein E, Bonet E, Dupuis V (2006), "Magnetic anisotropy of Co_xPt_{1-x} clusters embedded in a matrix: Influences of the cluster chemical composition and the matrix nature," *Phys. Rev. B*, vol. 74, 104408, doi: 10.1103/PhysRevB.74.104408.

Sander D (1999), "The correlation between mechanical stress and magnetic anisotropy in ultrathin films," *Rep. Prog. Phys.*, vol. 62, pp. 809–858, doi: 10.1088/0034-4885/62/5/204.

Seo W S, Lee J H, Sun X, Suzuki Y, Mann D, Liu Z, Terashima M, Yang P C, Mcconnell M V, Nishimura D G, Dai H (2006), "FeCo/graphitic-shell nanocrystals as advances magnetic-resonance-imaging and near-infrared agents," *Nature Mater.*, vol. 5, pp. 971–976, doi: 10.1038/nmat1775.

Skomski R and Coey J M D (1999), *Permanent Magnetism*, Bristol, U.K.: Inst. Phys. [Online]. Available: https://trove.nla.gov.au/version/7271414

Srikanth H (2019), "Tuning magnetic anisotropy in nanostructures for biomedical and electromagnetic applications," in *Proc. Int. Conf. Fine Particle Magn.*, M Rivas, P Corria, and J A Blanco, Eds., Gijón, Spain, May 2019, Paper 16.

Zeng H, Li J, Liu J P, Wang Z L, Sun S (2002), "Exchange-coupled nanocomposite magnets by nanoparticle self-assembly," *Nature*, vol. 420, pp. 395–398, doi:10.1038/nature01208.